Processing and Application of Ceramics 17 [4] (2023) 410–420
https://doi.org/10.2298/PAC2304410Y

Tailoring multifunctional performance of Dy-doped $(Ba_{0.85}Ca_{0.15})(Zr_{0.1}Ti_{0.9})O_3$ ceramics via optimizing ceramic processing

Yawen Yang[1], Zipeng Yan[1], Guangye Qiu[1], Bijun Fang[1,*], Shuai Zhang[1], Xiaolong Lu[1], Jianning Ding[1,2,*]

[1]*School of Materials Science and Engineering, Jiangsu Collaborative Innovation Center of Photovoltaic Science and Engineering, Jiangsu Province Cultivation Base for State Key Laboratory of Photovoltaic Science and Technology, National Experimental Demonstration Center for Materials Science and Engineering, Changzhou University, Changzhou 213164, China*
[2]*School of Mechanical Engineering, Yangzhou University, Yangzhou 225127, China*

Received 24 August 2023; Received in revised form 29 November 2023; Accepted 8 December 2023

Abstract

Dy-doped $(Ba_{0.85}Ca_{0.15})(Zr_{0.1}Ti_{0.9})O_3$ ($[(Ba_{0.85}Ca_{0.15})_{0.99}Dy_{0.01}](Zr_{0.1}Ti_{0.9})O_3$, 0.01Dy-BCZT) lead-free multifunctional ceramics were prepared by conventional solid-state sintering method, in which the effects of ceramic processing conditions were studied by structural analysis and performance characterization. The sintered 0.01Dy-BCZT ceramics have pure perovskite phase with composition near morphotropic phase boundary alongside apparent tetragonal distortion, high density and densified micro-morphology obtained via tailoring calcination and sintering temperatures. High resistivity, excellent dielectric performance and piezoelectricity were acquired, which were affected greatly by ceramic processing conditions. All samples exhibit excellent ferroelectric and strain properties, which approach intrinsic physical performance and have little dependency on ceramic processing conditions. Appearance of a strong broad emission peak, centred at ~442 nm, is related to the $^4F_{9/2} \rightarrow {}^6H_{15/2}$ electron transition. Strong piezoelectric-fluorescent coupling effect was produced due to adding Dy and using BCZT piezoelectric matrix, which provides a promising choice in optoelectronic application field.

Keywords: *Dy-doped BCZT, ceramic processing condition, electrical property, fluorescence performance*

I. Introduction

With the rapid development of optoelectronic science and technology, multifunctional materials have attracted worldwide research attention [1,2]. Among versatile optoelectronic devices, piezoelectric-fluorescent materials provide a prospect choice, where rare-earth metals doped piezoelectric ceramics are the most convenient and feasible option. With adding appropriate amount of rare-earth metal, electrical performance can be improved, fluorescence can be excited by fluorescent centre and strong piezoelectric-fluorescent coupling effect can be produced due to remnant polarization of ferroelectric and rare-earth doping induced photoluminescence performance [3–5]. In addition, high mechanical performance, wide band gap, low optical loss and high chemical and thermal stability can be acquired as well.

In this subject, lead-free piezoelectric materials are highly important for green development and environmentally friendly consideration since the main raw material, Pb-based oxide, for $Pb(Zr_{1-x}Ti_x)O_3$ (PZT)-based piezoelectric ceramics is harmful to health and environment [6]. $Ba(Zr_{0.2}Ti_{0.8})O_3$-$x(Ba_{0.7}Ca_{0.3})TiO_3$ (BCZT) system created a significant milestone in lead-free piezoelectric systems, and the obtained ultra-high piezoelectric constant d_{33} of 620 pC/N surpassed most PZT-based piezoelectric ceramics [7]. The large d_{33} value was firstly considered as correlating with "morphotropic phase boundary (MPB) with tricritical point", and was subsequently confirmed to be related to the orthogonal-tetragonal phase coexistence [8–10], inducing amazing application potential. Therefore, BCZT was selected

*Corresponding author: tel: +86 519 86330095,
e-mail: *fangbj@cczu.edu.cn* (B. Fang)
dingjn@cczu.edu.cn (J. Ding)

as phosphor matrix in this work, and the composition $(Ba_{0.85}Ca_{0.15})(Zr_{0.1}Ti_{0.9})O_3$ was chosen based on literature reports [7–10] and our previous research [11].

There are rich rare-earth resources, which are easily doped into ferroelectric matrix via mature ceramic processing and provide diversified options as fluorescent centre [12–14]. Dy^{3+} has outer electron configuration of $4f^9$, which emits strong yellow light, and weak blue and red light in visible light region due to the *f-f* electron transitions [15–17]. Since fluorescence emission is affected greatly by matrix coordination environment, white light fluorescence can be obtained by combining Dy^{3+} ion doping and substrate structure [15,16]. Therefore, the highly efficient activator ion dysprosium presents interesting applications in white light-emitting diodes, high brightness displays, laser emitters, etc., and was chosen as luminescence centre and generated multifunctional performance [18]. In this work Dy^{3+} doping concentration was maintained as 1 mol%, which balanced piezoelectric and fluorescent performance, located near concentration quenching amount, and aimed to study the change of multifunctional performance caused by varying ceramic processing conditions.

Conventional ceramic processing provides an effective and convenient method to fabricate rare-earth doped ferroelectric ceramics. Since the four elements of materials science have intimate correlation with each other, the study of ceramic processing condition is important due to the great influence on physical performance [19,20]. For the BCZT system, calcination temperature is especially essential, which affects the decomposition of carbonates and subsequent sintering behaviour.

In this paper, 1 mol% Dy-doped $(Ba_{0.85}Ca_{0.15})(Zr_{0.1}Ti_{0.9})O_3$ ceramics were prepared by solid-state sintering method and detailed study was conducted to find optimal calcination temperature and subsequent sintering conditions for good multifunctional performances. Due to the utilization of Dy-doping and BCZT ferroelectric matrix, strong piezoelectric-fluorescent coupling effect was produced, which would help to develop novel multifunctional material for optoelectronic application.

II. Experimental

High purity carbonates and oxides, $BaCO_3$, $CaCO_3$, ZrO_2, TiO_2 and Dy_2O_3, were used to prepare Dy-doped $(Ba_{0.85}Ca_{0.15})(Zr_{0.1}Ti_{0.9})O_3$ ceramics according to chemical formula $[(Ba_{0.85}Ca_{0.15})_{0.99}Dy_{0.01}](Zr_{0.1}Ti_{0.9})O_3$ (0.01Dy-BCZT) by conventional solid-state sintering technique. After sufficient drying, accurately weighted raw materials were fully ground and mixed, and then calcined at 1200 °C and 1300 °C for 4 h, separately. The calcined powders were ground and passed through 100 mesh sieve. Green pellets with diameter of 12 mm were pressed by uniaxial pressing under 400 MPa after granulation with addition of appropriate amount of the 5 wt.% polyvinyl alcohol (PVA) aqueous solution. The PVA binder was burned out separately at 600 °C for 2 h, then sintering was carried out at different temperatures for 3 h (Table 1) using the calcined powder covering pellets in sealed alumina crucible. The sintered samples have notation 0.01Dy-BCZT-1200 and 0.01Dy-BCZT-1300 corresponding to the calcination temperature of 1200 and 1300 °C, respectively.

Crystal structure of the well-polished sintered 0.01Dy-BCZT ceramics was characterized by Rigaku D/max-2500/PC X-ray diffractometer and its free surface morphology was observed by JEOL JSM-6510 scanning electron microscopy (SEM). Fluorescent performance was measured by Edinburgh FS5 Spectrometer.

Silver electrodes were printed and fired on the surface of the sintered 0.01Dy-BCZT ceramics. Resistance was measured by Agilent 4339B Meter, temperature dependent dielectric performance was characterized using Partulab HDMS-1000 attached to Microtest LCR Meter 6630-10, ferroelectric performance and strain were detected by Radiant Precision Premier LC II combined with SP-S 120 Laser interferometer, and piezoelectric performance was measured by ZJ-6A meter and TH2826 LCR Meter after samples were poled by MPD PLUS Multichannel Oil-Bath High Voltage Polarization Device [21].

III. Results and discussion

3.1. XRD analyses

Figure 1 compares influence of calcination and sintering temperatures on crystal structure of the prepared 0.01Dy-BCZT ceramics. All ceramics have rather pure perovskite structure, matching well with the standard material $(Ba_{0.91}Ca_{0.09})(Zr_{0.05}Ti_{0.95})O_3$ with PDF card 56-1033, confirming formation of solid solution. As compared with the standard material, Ti content is decreased slightly and additional Dy is added, thus the crystal structure would change accordingly. From Fig. 1 it can be seen that (001) and (100), (002) and (200) etc. present doublet splitting XRD peaks, revealing the existence of tetragonal phase symmetry. (211), (310) etc. show broad singlet XRD peak, and (311) exhibits doublet splitting trend, proving the rhombohedral phase symmetry. Therefore, the 0.01Dy-BCZT is still located around the well-known MPB region [7–10] and Dy doping can stabilize tetragonal symmetry. With the change of calcination and sintering temperatures, the doublet splitting characteristic and reflection peak intensity ratio change slightly, but cannot be distinguished in the whole XRD patterns.

Lattice parameters calculation can clearly show the influence of calcination and sintering temperatures on crystal structure. Based on Jade full crystal structure refinement, and indexed according to the tetragonal symmetry, cell parameters are calculated and shown in Table 1 combined with density data obtained by water im-

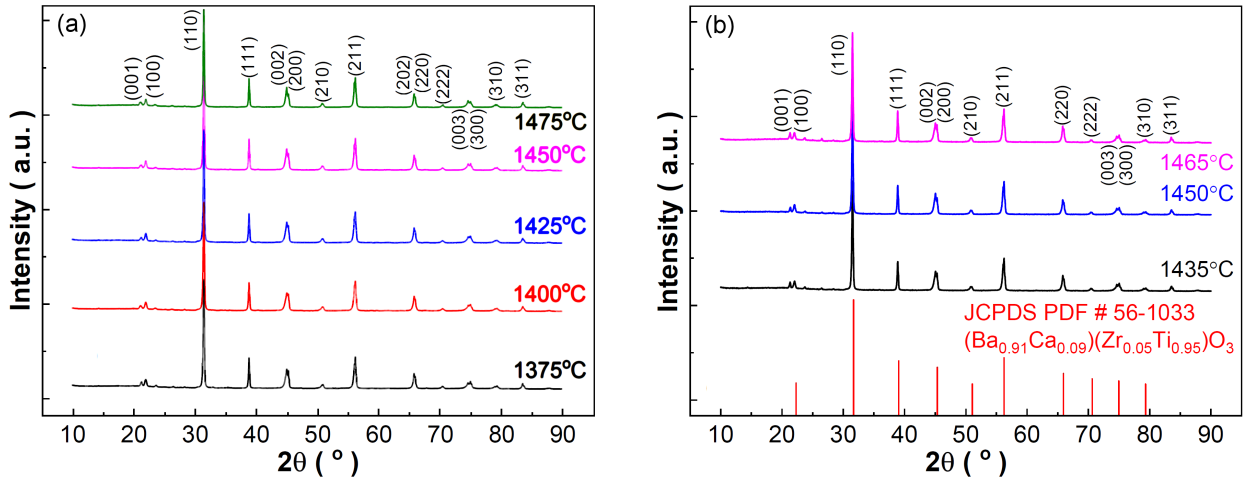

Figure 1. XRD patterns of prepared ceramics sintered at different temperatures for 3 h: a) 0.01Dy-BCZT-1200 and b) 0.01Dy-BCZT-1300

Table 1. Lattice parameters, theoretical volume V_{th}, bulk density ρ, theoretical density ρ_{th}, relative density ρ_r and resistivity of 0.01Dy-BCZT ceramics calcined and sintered at different temperatures

Calcination temperature [°C]	Sintering temperature [°C]	$a = b$ [Å]	c [Å]	V_{th} [Å^3]	c/a	ρ [g/cm^3]	ρ_{th} [g/cm^3]	ρ_r [%TD]	Resistivity [Ω·cm]
1200	1375	3.99900	4.02030	64.29	1.0053	5.440	5.7688	94.30	6.38×10^{11}
	1400	3.99840	4.01770	64.23	1.0048	5.555	5.7742	96.29	2.55×10^{11}
	1425	3.99960	4.01850	64.28	1.0047	5.559	5.7697	96.37	2.54×10^{11}
	1450	3.99810	4.01930	64.25	1.0053	5.457	5.7724	94.59	2.00×10^{11}
	1475	3.99750	4.02060	64.25	1.0058	5.467	5.7724	94.76	1.52×10^{11}
1300	1435	4.00032	4.01937	64.32	1.0048	5.280	5.5745	94.72	1.96×10^{11}
	1450	4.00002	4.01978	64.32	1.0049	5.470	5.5745	98.13	1.79×10^{12}
	1465	4.00069	4.01932	64.33	1.0047	5.220	5.5737	93.65	1.51×10^{11}

mersion measurement and theoretical density calculation [14]. Due to the coexistence of multiple ferroelectric phases, the tetragonality c/a is small for all samples, presenting slight variation around 1.005. a and b cell parameters are slightly larger, c cell parameter tends to be slightly smaller, and cell volume is slightly larger for the 0.01Dy-BCZT-1300 ceramics as compared to the 0.01Dy-BCZT-1200 ceramics. Cell parameters change little, especially in cell volume, as sintering temperature increases, whereas density presents apparent change. Optimized sintering temperature and sintering temperature range can be observed. For the 0.01Dy-BCZT-1200 samples, the largest relative density of 96.37% is obtained after sintering at 1425 °C; as comparison, for the 0.01Dy-BCZT-1300 samples, the largest relative density of 98.13% is obtained after sintering at 1450 °C. Such phenomenon is related mainly to the driving force variation provided by heating, decomposition difference of carbonates calcined at different temperatures and grain growth change induced by Dy-doping [19,20,22].

3.2. Microstructure characterization

The high densification is confirmed by SEM image shown in Fig. 2 using the 0.01Dy-BCZT-1200 sample sintered at 1425 °C as an example. Highly densified ceramics is observed clearly, where grains pack closely, grain boundary is visible clearly and almost no enclosed pores appear. Due to the Dy-doping, grain growth is inhibited to some extent, since grain size can reach dozens micron for the undoped BCZT ceramics prepared by solid-state method [23], whereas grain size tends to have bimodal distribution in the BCZT ceramics prepared via liquid-phase method [24]. Most grains have irregular polyhedral shape, revealing that main densification mechanism comes from solid-state sintering [7,10] and preparation of the $BaTiO_3$-based ceramics requires high sintering temperature and high energy consumption. The grain size distributions with good statistical reliability were obtained from two photos containing a large number of grains. Although it looks like bimodal distribution of grain size, a nearly normal distribution curve is obtained for the grain size distribution. Most grains have grain size of 11.9–16.5 μm and the average grain size is 13.0 μm. Relatively small grain sizes are comparable with the data reported by Chandrakala *et al.* [24] for $0.5Ba(Zr_{0.2}Ti_{0.8})O_3$-$0.5(Ba_{0.7}Ca_{0.3})TiO_3$ ceramics (with the same composition of the undoped matrix) derived via sol-gel route and sintered at 1550 °C for 2 h (having densification of ~97% and grain size

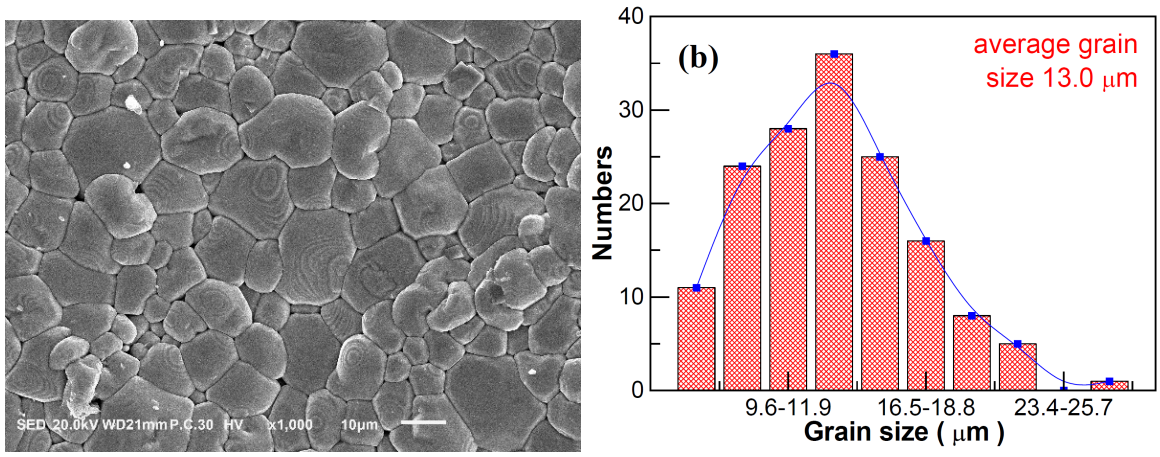

Figure 2. SEM image (a) and grain size distribution (b) of 0.01Dy-BCZT-1200 ceramics sintered at 1425 °C for 3 h

of ~10 μm). In a similar system, He *et al.* [3] reported the average grain size from 210 nm to 330 nm for the $[(Ba_{0.85}Ca_{0.15})_{0.995}Nd_{0.005}](Ti_{0.9}Hf_{0.1})O_3$ ceramics prepared via hydrothermal method and sintered at 1180–1260 °C for 2–18 h. However, the decreased grain size would hamper piezoelectric performance as reported before [23].

3.3. Resistance and dielectric performance

Insulation is crucial performance for any electronic-related application field [21]. As shown in Table 1, resistivity of the 0.01Dy-BCZT-1200 ceramics decreases gradually with increasing sintering temperature, whereas, resistivity increases at first and then decreases with increasing sintering temperature for the 0.01Dy-BCZT-1300 samples. For the ceramics sintered at the same temperature of 1450 °C, the resistivity of 1.79×10^{12} Ω·cm of the 0.01Dy-BCZT-1300 sample is larger than that of the 0.01Dy-BCZT-1200 sample with 2.00×10^{11} Ω·cm, being consistent with corresponding relative density. For other samples, the resistivity is slightly lower for the 0.01Dy-BCZT-1300 ceramics. All ceramics have high resistivity, all larger than 10^{11} Ω·cm, partially related to the high density, small porosity, and relatively homogenous microstructure [21].

Figure 3 shows temperature dependent dielectric properties of the 0.01Dy-BCZT ceramics using 1 kHz data to compare the effect of calcination and sintering temperatures. All samples present sole dielectric anomaly peak, corresponding to the Curie temperature T_C, related to the MPB ferroelectric phase to cubic paraelectric phase transition [25]. For the 0.01Dy-BCZT-1200 samples, besides the ceramics sintered at 1375 °C, dielectric constant and the maximum value ε_m increase, T_C increases, and dielectric peak becomes narrower with elevating sintering temperature. As comparison, for the 0.01Dy-BCZT-1300 samples, the ceramics sintered at 1450 °C has the largest ε_m and T_C values, partially correlating with the largest relative density. Overall, most 0.01Dy-BCZT ceramics exhibit excellent dielectric performance, which can be attributed to the MPB effect due to the composition selected in this work [26,27], and tailored ceramic processing [20].

Frequency dependent dielectric properties can be used to determine type of ferroelectric behaviour [28]. As can be seen from Fig. 4 of two samples with maximum density in each system, both samples have rather broad dielectric anomaly peak. The 0.01Dy-BCZT-1300

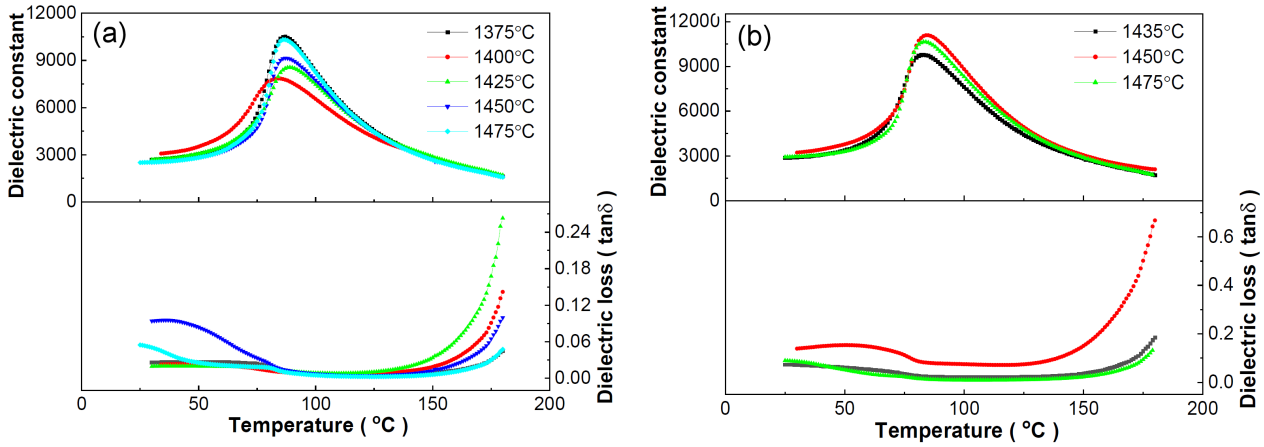

Figure 3. Dielectric performance-temperature relationship at 1 kHz upon heating of prepared ceramics sintered at different temperatures for 3 h: a) 0.01Dy-BCZT-1200 and b) 0.01Dy-BCZT-1300

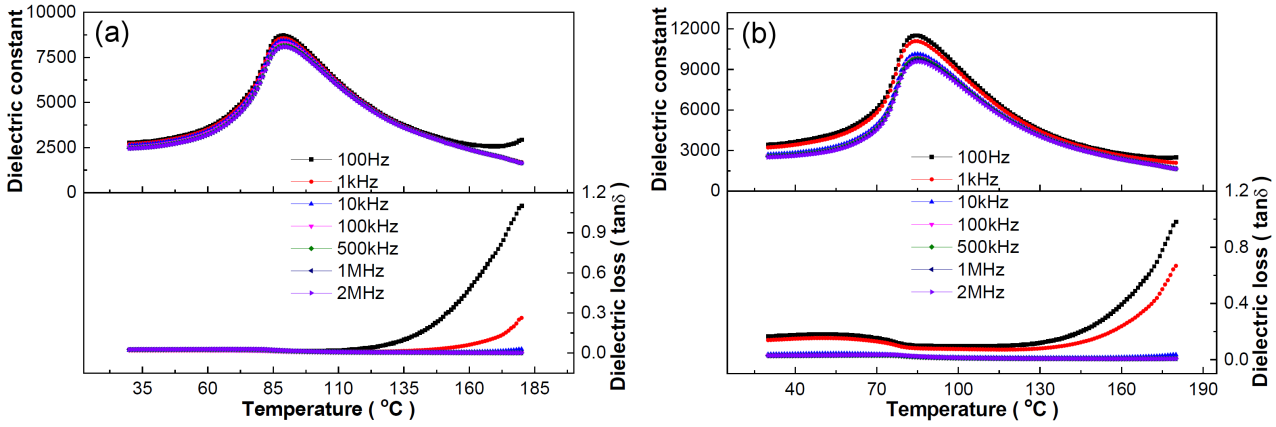

Figure 4. Dielectric property-temperature relationship measured at several frequencies upon heating of 0.01Dy-BCZT ceramics with maximum density: a) 0.01Dy-BCZT-1200 sintered at 1425 °C and b) 0.01Dy-BCZT-1300 sintered at 1450 °C

sample sintered at 1450 °C has apparent dielectric frequency dispersion, from room temperature to temperatures higher than the T_C. On the other hand, frequency dispersion is slightly visible just around the T_C temperature for the 0.01Dy-BCZT-1200 ceramics sintered at 1425 °C.

Figures 3 and 4 confirm that all samples have abnormally large dielectric loss high above the TC temperature, especially at low frequency. Such rapid increase of loss tangent is caused by point defects conduction [29] due to the evaporation of some metals during high-temperature sintering and Dy substitution at the A-site of perovskite structure, which produce oxygen vacancies as shown below [30,31]:

$$Ba_{Ba}^{x} + O_{O}^{x} \longrightarrow Ba\uparrow + 0.5\,O_2\uparrow + V_{Ba}'' + V_{O}^{\bullet\bullet} \quad (1)$$

$$Ca_{Ca}^{x} + O_{O}^{x} \longrightarrow Ca\uparrow + 0.5\,O_2\uparrow + V_{Ca}'' + V_{O}^{\bullet\bullet} \quad (2)$$

$$Dy_2O_3 \xrightarrow{BCZT} 2\,Dy_{Ba/Ca}^{\bullet} + V_{Ba/Ca}'' + O_{O}^{x} \quad (3)$$

Such lossy conduction belongs to the thermal activation type and has hopping-jumping movement characteristic, which induces large dielectric loss at elevated temperatures and can be confirmed indirectly by impedance conduction analysis [21,32].

The ferroelectrics type is studied further by dielectric performance behaviour fitting using two laws [21,31,33] Curie-Weiss law:

$$\varepsilon = \frac{C}{T - T_0} \quad (4)$$

and exponential law:

$$\frac{1}{\varepsilon} - \frac{1}{\varepsilon_m} = \frac{(T - T_m)^{\gamma}}{C'} \quad (5)$$

The fitting results are shown in Fig. 5 for two samples with maximum density in each system as examples. For the 0.01Dy-BCZT-1200 ceramics sintered at 1425 °C, the Curie-Weiss law fitting gives $\varepsilon = 1.86 \times 10^5/(T - 83.6)$, in which the temperature begins to obey the Curie-Weiss law at $T_{cw} = 115$ °C. The exponential law fitting result for the same sample is $1/\varepsilon - 1/8557.95 = (T - 89)^{1.539}/(2.14 \times 10^6)$, in which the diffusive coefficient $\gamma = 1.539$. For the 0.01Dy-BCZT-1300 ceramics sintered at 1450 °C, the Curie-Weiss law fitting result gives $\varepsilon = 1.66 \times 10^5/(T - 90.9)$, in which $T_{cw} = 127$ °C. The exponential law fitting result for the same sample is $1/\varepsilon - 1/10136 = (T - 85)^{1.539}/(2.14 \times 10^6)$, in which $\gamma = 1.539$. Above the T_{cw} temperature, the ferroelectric phase transition from MPB ferroelectric phase to cubic paraelectric phase occurs completely [25]. Both ceramics have Curie-Weiss constant C in the 10^5 order, whereas $T_{cw} - T_m$ is 26 °C and 42 °C, and temperature range obeying the Curie-Weiss law is 115–170 °C and 127–168 °C, respectively. These results confirm that the ferroelectric phase transition is driven by displacement transition accompanied by apparent deviation [21,31,33]. Both γ values are slightly larger than 1.5 but less than 2, indicating that both samples have obvious relaxation characteristic, but are not typical relaxor ferroelectrics. The relaxation behaviour is normally attributed to the formation of polar clusters or nanoregions, and the crystal cell distortion caused by multiple ions substitution at A-site and/or B-site of the perovskite structure [34]. Therefore, all 0.01Dy-BCZT ceramics have complicate dielectric performance with behaviour of normal ferroelectrics accompanied by apparent dispersion behaviour and relaxation characteristic.

3.4. Ferroelectric performance

Figure 6 shows polarization-electric field (*P-E*) hysteresis loops and strain-electric field (*S-E*) butterfly-like loops of the 0.01Dy-BCZT ceramics prepared under different conditions. All ceramics exhibit rather narrow, slender and easily saturated *P-E* loops, corresponding well with the composition near the MPB region confirmed by XRD analysis and high relaxation behaviour revealed by dielectric performance characterization. Calcination and sintering temperatures have little influence on ferroelectric properties, indicating that ferroelectricity is mainly related to chemical composi-

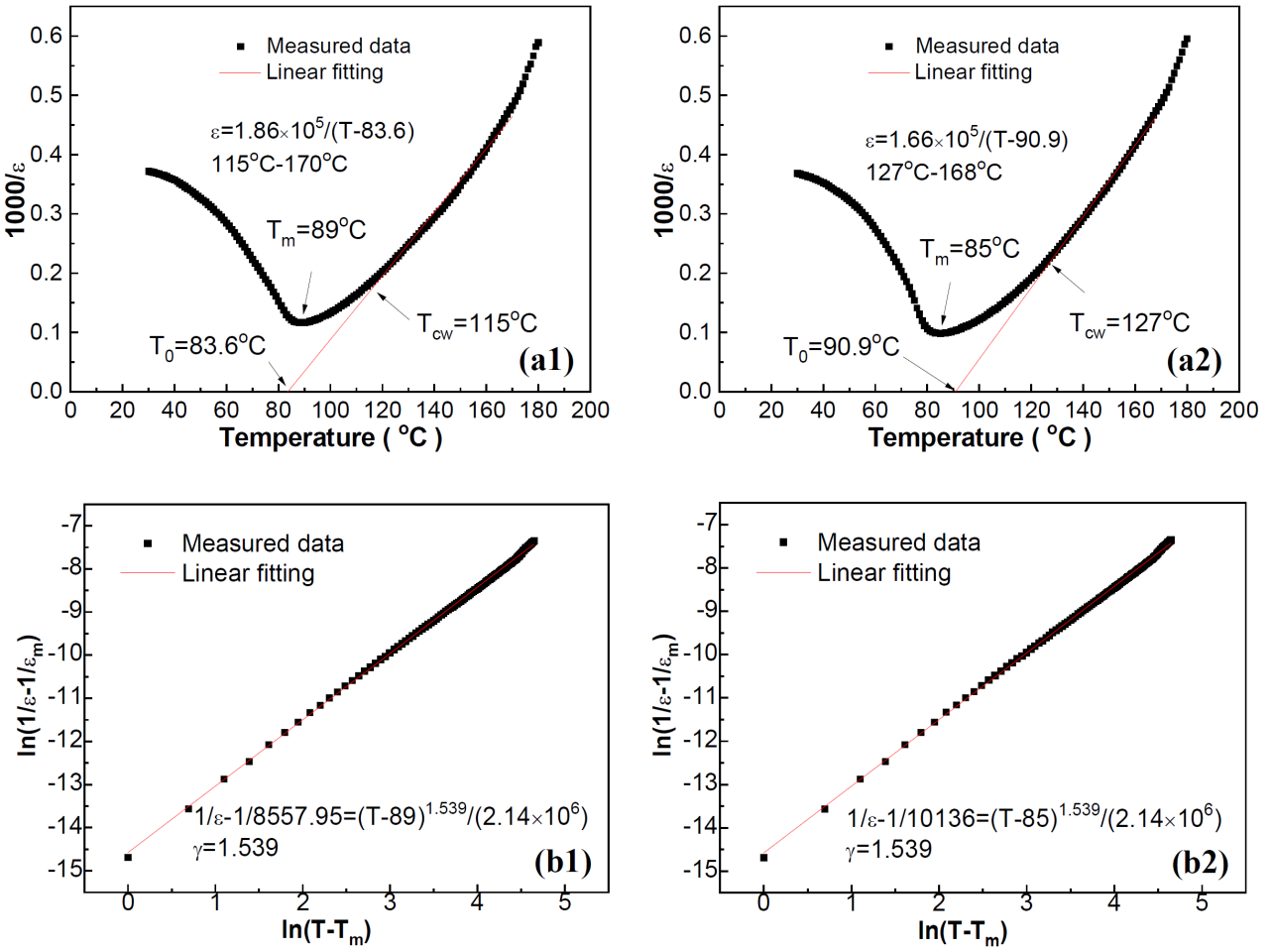

Figure 5. Dielectric performance fitting (the Curie-Weiss law (a) and exponential law (b)) above T_C temperature of prepared ceramics using 1 kHz data for 0.01Dy-BCZT-1200 sintered at 1425 °C (1) and 0.01Dy-BCZT-1300 sintered at 1450 °C (2)

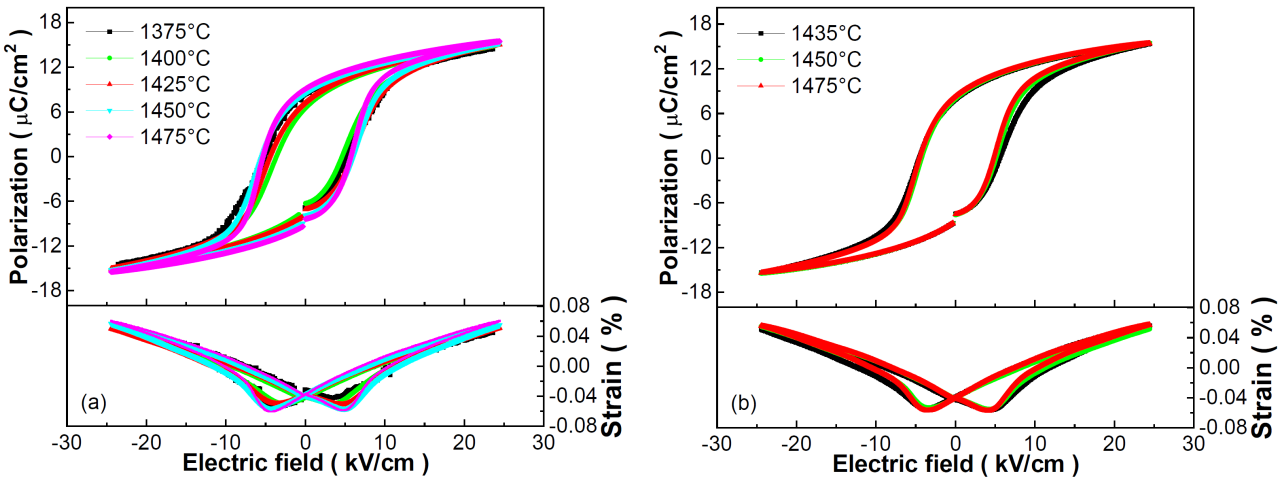

Figure 6. *P-E* and *S-E* curves of prepared ceramics sintered at different temperatures: a) 0.01Dy-BCZT-1200 and b) 0.01Dy-BCZT-1300

tion and belongs to intrinsic physical performance in this work [35]. *S-E* loops exhibit typical butterfly-like shape, with maximum strain of ~0.06% at 25 kV/cm. As compared with the undoped BCZT ceramics, remnant polarization P_r decreases slightly from 10.44 μC/cm^2 to ~9.2 μC/cm^2 [11], and coercive electric field E_c nearly doubles from 2.768 kV/cm to ~5.3 kV/cm. These changes are attributed to the Dy doping and pinning-down effect caused by metal evaporation during sintering and donor point defect due to Dy substitution at the A-site of perovskite structure as discussed above [29–31].

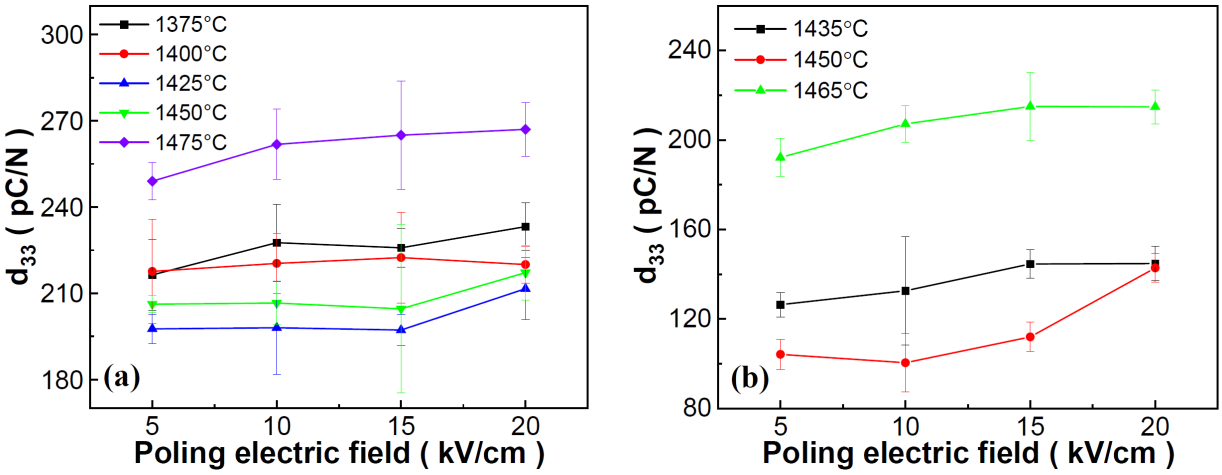

Figure 7. Piezoelectricity-electric field curves of prepared ceramics sintered at different temperatures: a) 0.01Dy-BCZT-1200 and b) 0.01Dy-BCZT-1300

3.5. Piezoelectric performance

Figure 7 shows influence of electric field on piezoelectric constant d_{33} of the 0.01Dy-BCZT ceramics prepared under different conditions. Even though they are poled at only 5 kV/cm, all samples present considerable piezoelectricity, especially for the 0.01Dy-BCZT-1200 ceramics, matching well with the low E_c value and showing soft piezoelectric material characteristics [11,30]. With the increase of electric field, the d_{33} value continues to increase slightly in almost linear trend, and can be larger than 200 pC/N for most samples. For the two systems calcined at different temperatures, the ceramics sintered at respectively the highest temperature present the largest d_{33} value, which is related to the contribution of large grain size to piezoelectric performance in the BCZT system [24]. The maximal d_{33} values reach 267 and 215 pC/N for the 0.01Dy-BCZT-1200 ceramics sintered at 1475 °C and the 0.01Dy-BCZT-1300 ceramics sintered at 1465 °C, respectively.

Figure 8 shows frequency dependent impedance Z^* and phase angle θ of the 0.01Dy-BCZT ceramics with maximum density in each system poled at 20 kV/cm. Rather perfect resonance curves are obtained in both samples related to good circularity of ceramics and indicating high energy conversion efficiency. The θ value varies from −89° to 76.5° for the 0.01Dy-BCZT-1200 sample sintered at 1425 °C, and from −88.8° to 57.8° for the 0.01Dy-BCZT-1300 sample sintered at 1450 °C. Such change of the θ value shows that the poling behaviour of the ceramics can be improved further via improving ceramics' quality and tailoring poling conditions since fully poled samples typically have θ value ranging from −90° to +90° [36,37]. Based on the above results, electromechanical coupling factor K_p, mechanical quality factor Q_m and frequency constant N_p are calculated according to following equations:

$$K_p \approx \sqrt{\frac{f_p - f_s}{f_s} \cdot 2.33} \tag{6}$$

$$Q_m = \frac{f_p^2}{2\pi \cdot f_s \cdot C^T \cdot R(f_p^2 - f_s^2)} \tag{7}$$

$$N_p = f_s \cdot d \tag{8}$$

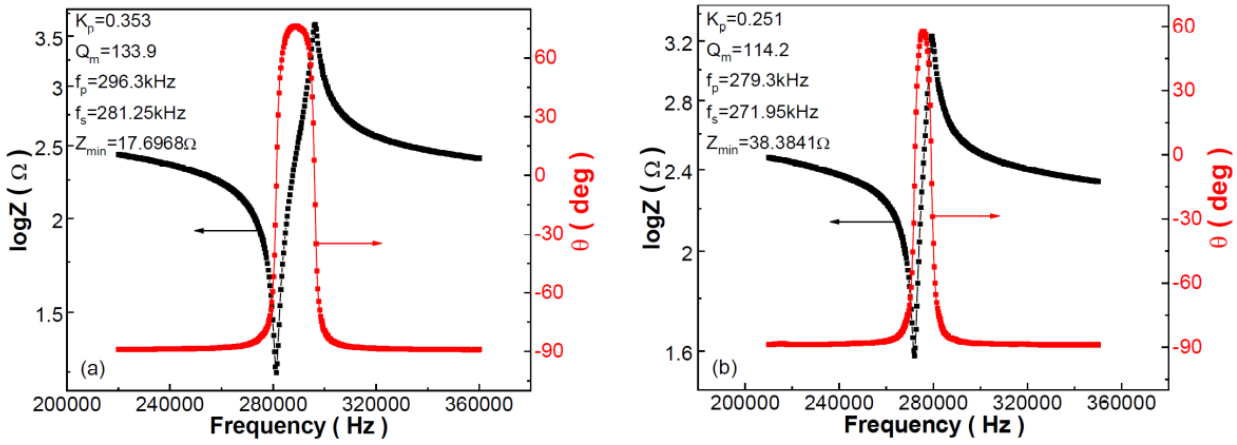

Figure 8. Change of impedance and phase angle with frequency for prepared ceramics with maximum density poled at 20 kV/cm: a) 0.01Dy-BCZT-1200 sintered at 1425 °C and b) 0.01Dy-BCZT-1300 sintered at 1450 °C

Table 2. Lattice parameters, theoretical volume V_{th}, bulk density ρ, theoretical density ρ_{th}, relative density ρ_r and resistivity of 0.01Dy-BCZT ceramics calcined and sintered at different temperatures

Calcination temperature [°C]	Sintering temperature [°C]	d_{33} [pC/N]	d^*_{33} [pm/V]	g_{33} [$\times 10^{-3}$ V·m/N]	K_p	Q_m	N_p [Hz·m]
1200	1375	233 ± 8.3	304.8	9.79	0.278	101.6	2986.9
	1400	220 ± 6.4	378.0	8.08	0.288	110.6	2980.9
	1425	212 ± 10.8	332.6	8.91	0.353	133.9	2947.5
	1450	217 ± 9.5	373.8	9.73	0.361	138.6	2920.1
	1475	267 ± 9.5	394.9	12.05	0.407	124.3	2887.0
1300	1435	145 ± 7.6	368.0	5.69	0.325	111.4	2936.6
	1450	143 ± 6.4	351.4	5.01	0.251	114.2	2920.7
	1465	215 ± 7.6	405.8	8.30	0.301	108.4	2934.4

The calculated data are shown in Table 2 combined with piezoelectricity, in which converse piezoelectric coefficient d^*_{33} is obtained based on the *S-E* curves, and piezoelectric voltage coefficient g_{33} is defined by following equation [24]:

$$g_{33} = \frac{\varepsilon_{33}}{\varepsilon_0 \cdot \varepsilon_r} \tag{9}$$

Although complicated change trend appears in the above performance, d_{33}, d^*_{33} and K_p tend to present excellent performance at the respectively highest sintering temperature.

3.6. Fluorescence performance

Due to the *f-f* electron transitions of Dy^{3+} [15–17] and ultra-high piezoelectricity of BCZT [7–10], strong photoluminescent performance and piezoelectric-fluorescent coupling effect are generated in the 0.01Dy-BCZT samples. Figure 9a shows excitation spectra of the 0.01Dy-BCZT ceramics with maximum density monitored at 550 nm. Both samples have similar shape of excitation spectra, where a broad excitation peak and an excitation peak shoulder centre at ~295 nm and ~345 nm are related to the $^6H_{15/2} \rightarrow {}^6P_{3/2}$ and $^6H_{15/2} \rightarrow {}^4I_{13/2}$ electron transitions, respec-

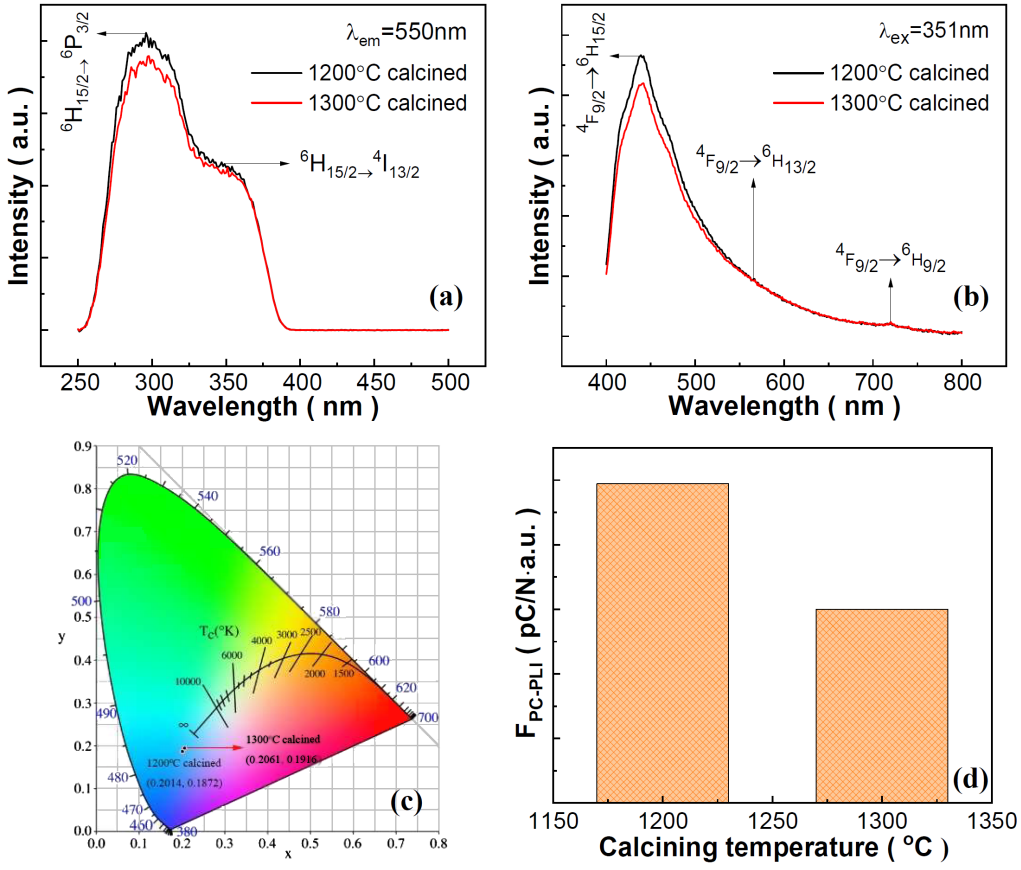

Figure 9. Fluorescence related performance of 0.01Dy-BCZT-1200 sample sintered at 1425 °C and 0.01Dy-BCZT-1300 sample sintered at 1450 °C: a) excitation spectra, b) emission spectra, c) CIE1931 chromaticity coordinate diagram and d) figure of merit for piezoelectric-fluorescent coupling effect

Table 3. Fluorescence performance for 0.01Dy-BCZT ceramics with maximum density

Ceramic processing condition	Chromaticity coordinate	*CP* [%]	*CCT* [K]
0.01Dy-BCZT-1200 sintered at 1425 °C	(0.2014, 0.1872)	63.36	1903
0.01Dy-BCZT-1300 sintered at 1450 °C	(0.2061, 0.1946)	60.58	1851

tively [15–17]. The excitation intensity of the 0.01Dy-BCZT-1200 sample is generally larger than that of the 0.01Dy-BCZT-1300 sample.

Figure 9b shows emission spectra the 0.01Dy BCZT ceramics excited at 351 nm. Unlike ordinary phosphor, a lower energy light with wavelength of 351 nm near the excitation peak shoulder can excite the Dy-based phosphor. Then, a strong broad emission peak appears centred at ~442 nm, which is attributed to the $^4F_{9/2} \rightarrow {}^6H_{15/2}$ electron transition. Two weak emission peaks, centred at ~565 nm relating to $^4F_{9/2} \rightarrow {}^6H_{13/2}$ and at ~720 nm related to $^4F_{9/2} \rightarrow {}^6H_{9/2}$, are generated, presenting great dependency on Dy doping concentration and ceramic processing conditions [15–17]. The 0.01Dy-BCZT-1200 sample also exhibits larger emission intensity as compared to the 0.01Dy-BCZT-1300 sample. The increased emission intensity indicates greater energy absorption in certain energy band and shows higher energy utilization efficiency.

Figure 9c shows CIE1931 chromaticity diagram of the 0.01Dy BCZT ceramics excited at 351 nm, which provides important parameter for colour coordinate and colour purity, and evaluates practical application possibility for phosphors [15]. The chromaticity coordinate is (0.2014, 0.1872) for the 0.01Dy-BCZT-1200 ceramics sintered at 1425 °C, and (0.2061, 0.1946) for the 0.01Dy-BCZT-1300 ceramics sintered at 1450 °C. Both samples emit similar coloured light, located at the junction region of blue and purple light, i.e. purplish blue, and having deviation from the standard blue light defined by the National Television Standards Committee with chromaticity coordinate of (0.1400, 0.0800). Table 3 displays fluorescence related performance of the 0.01Dy-BCZT ceramics calculated with following equations [15,38]:

$$CP = \sqrt{\frac{(x - x_i)^2 + (y - y_i)^2}{(x_d - x_i)^2 + (y_d - y_i)^2}} \cdot 100 \quad (10)$$

$$CCT = -449n^3 + 3525n^2 - 6823n + 5520.33 \quad (11)$$

Since the emitted light exhibits purplish blue colour, the calculated colour purity (*CP*) is rather low and the correlated colour temperature (*CCT*) is also not high.

For optoelectronic application, piezoelectric-fluorescent performance coupling effect is important, and a figure of merit, $F_{PC\cdot PLI} = d_{33} \cdot I_{PL}$, is proposed to evaluate the piezoelectric-fluorescent coupling effect as shown in Fig. 9d [3]. Since $F_{PC\cdot PLI}$ is a product property, it is required to balance piezoelectric constant and photoluminescence performance via tailoring composition and improving ceramic processing [3]. In this work, the 0.01Dy-BCZT-1200 ceramics sintered at 1425 °C shows relatively high $F_{PC\cdot PLI}$ merit value, presenting broad application prospect in the field of optoelectronics.

IV. Conclusions

High density and pure perovskite phase 0.01Dy-BCZT ceramics were prepared by conventional solid-state sintering method, where the influence of calcination and sintering temperatures on structure and multifunctional properties was studied in detail. The prepared 0.01Dy-BCZT ceramics are located around the MPB region with apparent tetragonal distortion, in which the ratio of rhombohedral and tetragonal phases and densification are affected by ceramic processing. The 0.01Dy-BCZT-1200 ceramics sintered at 1425 °C has densified microstructure with bimodal distribution of grain size and relatively small average grain size of 13.0 μm densified mainly through solid-state sintering mechanism. High insulation with resistivity larger than 10^{11} Ω·cm was obtained in all ceramics, where the 0.01Dy-BCZT-1300 sample sintered at 1450 °C has the largest resistivity of 1.79×10^{12} Ω·cm. Most 0.01Dy-BCZT ceramics exhibit excellent dielectric performance, presenting displacive transition ferroelectric accompanied by apparent dispersion behaviour and relaxation characteristics, and ε_m and T_C are affected greatly by ceramic processing conditions. Slender *P-E* loops and butterfly-like *S-E* curves are obtained in all samples, where P_r is ~9.2 μC/cm^2, E_c is ~5.3 kV/cm, and maximum strain is ~0.06% at 25 kV/cm. Rather well piezoelectric property and fluorescence performance are achieved simultaneously due to the utilization of Dy doping and BCZT ferroelectric matrix, resulting in strong piezoelectric-fluorescent coupling effect which presents broad application prospect in optoelectronic field.

Acknowledgement: This work was supported by the Top-notch Academic Programs Project of Jiangsu Higher Education Institutions and the Priority Academic Program Development of Jiangsu Higher Education Institutions.

References

1. J.E. Leal-Perez, J. Flores-Valenzuela, J.L. Almaral-Sánchez, R. Herrera-Basurto, J. González-Hernández, O. Auciello, A. Hurtado-Macías, "Cole-Cole analysis and optoelectronic properties, using VEELS, of KNNS ferroelectric ceramics", *Mater. Today Commun.*, **33** (2022) 104781.
2. M. Benaissa, W. Sigle, I. Benabdallah, R.T. ElAfandy, T.K. Ng, P.A. van Aken, "Optical properties of freestanding GaN nanomembranes using monochromated valence-

EELS", *Mater. Sci. Eng. B*, **272** (2021) 115333.
3. S. Zhang, B. Fang, S. Zhang, X. Lu, J. Ding, "Composition designing and sintering behavior tailoring in $[(Ba_{1-x}Ca_x)_{0.995}Eu_{0.005}](Ti_{1-y}Hf_y)O_3$ multifunctional piezoceramics", *J. Alloys Compd.*, **888** (2021) 160891.
4. C. Chen, X. Xia, L.Q. Zheng, L.H. Luo, N. Tu, Z.Y. Shen, X.P. Jiang, J.M. Liu, "Effects of phase structure on upconversion photoluminescence and dielectric performance in Er^{3+} doped $(Bi_{0.5}Na_{0.5})TiO_3$-$BaTiO_3$ lead-free ceramics", *J. Alloys Compd.*, **801** (2019) 619–625.
5. C.L. Ma, W.P. Zhou, Z.X. Gan, X.Y. Wang, W.S. Tan, Z.M. Zhang, Z.Y. Zhai, "Upconversion photoluminescence modulation by electric field poling in Er^{3+} doped $(Ba_{0.85}Ca_{0.15})(Zr_{0.1}Ti_{0.9})O_3$ piezoelectric ceramics", *J. Alloys Compd.*, **794** (2019) 325–332.
6. L. Chen, H. Liu, H. Qi, J. Chen, "High-electromechanical performance for high-power piezoelectric applications: Fundamental, progress, and perspective", *Prog. Mater. Sci.*, **127** (2022) 100944.
7. W. Liu, X. Ren, "Large piezoelectric effect in Pb-free ceramics", *Phys. Rev. Lett.*, **103** (2009) 257602.
8. H. Bao, C. Zhou, D. Xue, J. Gao, X. Ren, "A modified lead-free piezoelectric BZT-xBCT system with higher T_C", *J. Phys. D Appl. Phys.*, **43** (2010) 465401.
9. D.S. Keeble, F. Benabdallah, P.A. Thomas, M. Maglione, J. Kreisel, "Revised structural phase diagram of $(Ba_{0.7}Ca_{0.3}TiO_3)$-$(BaZr_{0.2}Ti_{0.8}O_3)$", *Appl. Phys. Lett.*, **102** (2013) 092903.
10. Y. Tian, X. Chao, L. Jin, L. Wei, P. Liang, Z. Yang, "Polymorphic structure evolution and large piezoelectric response of lead-free (Ba,Ca)(Zr,Ti)O_3 ceramics", *Appl. Phys. Lett.*, **104** (2014) 112901.
11. B.J. Fang, W.W. Wang, J.N. Ding, X.Y. Zhao, H.Q. Xu, H.S. Luo, "Preparation and electrical properties of pseudoternary $BaTiO_3$-$CaTiO_3$-$BaZrO_3$ lead free piezoelectric ceramics", *Adv. Appl. Ceram.*, **112** (2013) 257–262.
12. H.J. Wang, J.F. Lin, B.Y. Deng, T.F. Lin, C. Lin, Y. Cheng, X. Wu, X.H. Zheng, X. Yu, "Reversible multi-mode modulations of optical behavior in photochromic-translucent Nd-doped $K_{0.5}Na_{0.5}NbO_3$ ceramics", *J. Mater. Chem. C*, **8** (2020) 2343–2352.
13. J. Xu, Q. Lu, J. Lin, C. Lin, X. Zheng, T. Lin, X. Wu, "Enhanced ferro-/piezoelectric properties of tape-casting-derived Er^{3+}-doped $Ba_{0.85}Ca_{0.15}Ti_{0.9}Zr_{0.1}O_3$ optoelectronic thick films", *J. Adv. Ceram.*, **9** (2020) 693–702.
14. X. He, B. Fang, S. Zhang, X. Lu, J. Ding, "Preparation and properties of Nd-doped BCTH lead-free ceramics by solid-phase twin crystal method", *Curr. Appl. Phys.*, **38** (2022) 30–39.
15. Y. Zhang, Z. Liang, W. Wang, Y. Lin, R. Tang, J. Wang, D. He, J. Liu, Z. Zhang, L. Zhao, B. Deng, D. Zhang, R. Yu, "Optical properties of yellow-emitting $Sr_3LaNb_3O_{12}$:Dy^{3+} phosphors with an abnormal thermal quenching for white light-emitting diode applications", *J. Mater. Sci. Mater. Electron.*, **33** (2022) 26619–26632.
16. H. Li, W. Yang, Y. Lin, S. Ling, F. Xiong, "Preparation and luminescent properties of $Sr_7Sb_2O_{12}$:Dy^{3+} phosphors", *J. Synth. Crystals*, **51** (2022) 1921–1928.
17. S. Kumari, E. Sharma, J. Verma, J. Dalal, A. Kumar, "Structural and photoluminescence properties of Dy-doped nanocrystalline ZrO_2 for optoelectronics application", *Ceram. Int.*, **49** (2023) 20185–20192.
18. X. Qiao, A. Sheng, D. Wu, F. Zhang, B. Chen, P. Liang, J. Wang, X. Chao, Z. Yang, "A novel multifunctional ceramic with photoluminescence and outstanding energy storage properties", *Chem. Eng. J.*, **408** (2021) 127368.
19. L. Jiang, Z. Tan, L. Xie, Y. Li, J. Xing, J. Wu, Q. Chen, D. Xiao, J. Zhu, "Study of the relationships among the crystal structure, phase transition behavior and macroscopic properties of modified (K,Na)NbO_3-based lead-free piezoceramics", *J. Eur. Ceram. Soc.*, **38** (2018) 2335–2343.
20. M.A. Beuerlein, N. Kumar, T.-M. Usher, H.J. Brown-Shaklee, N. Raengthon, I.M. Reaney, D.P. Cann, J.L. Jones, G.L. Brennecka, "Current understanding of structure-processing-property relationships in $BaTiO_3$-$Bi(M)O_3$ dielectrics", *J. Am. Ceram. Soc.*, **99** (2016) 2849–2870.
21. Y. Zhou, B. Fang, S. Zhang, X. Lu, J. Ding, "Enhancing densification and electrical properties of KNN-based lead-free ceramics via two-step sintering", *J. Korean Chem. Soc.*, **59** (2022) 551–564.
22. J. Zidani, M. Zannen, M. Hadouchi, H.A.H. Alzahrani, E. Birks, H. Khemakhem, M. Majdoub, M. El Marssi, A. Lahmar, "Structural, electrical and optical properties of lanthanide-doped $Na_{0.4}K_{0.1}Bi_{0.5}TiO_3$ ceramics", *Physica B*, **653** (2023) 414680.
23. K. Castkova, K. Maca, J. Cihlar, H. Hughes, A. Matousek, P. Tofel, Y. Bai, Tim W. Button, "Chemical synthesis, sintering and piezoelectric properties of $(Ba_{0.85}Ca_{0.15})(Ti_{0.9}Zr_{0.1})O_3$ lead-free ceramics", *J. Am. Ceram. Soc.*, **98** (2015) 2373–2380.
24. E. Chandrakala, J. Paul Praveen, B.K. Hazra, D. Das, "Effect of sintering temperature on structural, dielectric, piezoelectric and ferroelectric properties of sol-gel derived BZT-BCT ceramics", *Ceram. Int.*, **42** (2016) 4964–4977.
25. K. Xu, J. Li, X. Lv, J. Wu, X. Zhang, D. Xiao, J. Zhu, "Superior piezoelectric properties in potassium-sodium niobate lead-free ceramics", *Adv. Mater.*, **28** (2016) 8519–8523.
26. S.R. Maity, B. Tiwari, M. Rath, M.S. Ramachandra Rao, "Composition-driven structural phase transition in ferroelectric $PbZr_xTi_{1-x}O_3$ across the morphotropic phase boundary", *J. Solid State Chem.*, **325** (2023) 124131.
27. S.-Y. Liu, Y. Meng, S. Liu, D.-J. Li, Y. Li, Y. Liu, Y. Shen, S. Wang, "Compositional phase diagram and microscopic mechanism of $Ba_{1-x}Ca_xZr_yTi_{1-y}O_3$ relaxor ferroelectrics", *Phys. Chem. Chem. Phys.*, **19** (2017) 22190–22196.
28. T. Zheng, J. Wu, D. Xiao, J. Zhu, "Recent development in lead-free perovskite piezoelectric bulk materials", *Prog. Mater. Sci.*, **98** (2018) 552–624.
29. Y. Wang, W. Jie, C. Yang, X. Wei, J. Hao, "Colossal permittivity materials as superior dielectrics for diverse applications", *Adv. Funct. Mater.*, **29** (2019) 1808118.
30. F.A. Kröger, H.J. Vink, "Relations between the concentrations of imperfections in crystalline solids", *Solid State Phys.*, **3** (1956) 307–435.
31. W. Ji, S. Feng, B. Fang, X. Zhao, S. Zhang, J. Ding, H. Luo, "Facile preparation and performance of novel high-T_C $xBi(Ni_{1/2}Ti_{1/2})O_3$-$(1-x)Pb(Zr_{1/2}Ti_{1/2})O_3$ piezoceramics", *Curr. Appl Phys.*, **18** (2018) 289–296.
32. L. Li, T. Roncal-Herrero, J. Harrington, S.J. Milne, A.P. Brown, J.S. Dean, D.C. Sinclair, "Anomalous grain boundary conduction in $BiScO_3$-$BaTiO_3$ high temperature dielectrics", *Acta Mater.*, **216** (2021) 117136.
33. K. Uchino, S. Nomura, "Critical exponents of the dielectric constants in diffused-phase-transition crystals", *Ferro-*

electr. Lett., **44** (1982) 55–61.
34. P. Li, Y. Huan, W. Yang, F. Zhu, X. Li, X. Zhang, B. Shen, J. Zhai, "High-performance potassium-sodium niobate lead-free piezoelectric ceramics based on polymorphic phase boundary and crystallographic texture", *Acta Mater.*, **165** (2019) 486–495.
35. F. Li, S. Zhang, Z. Xu, X. Wei, J. Luo, T.R. Shrout, "Composition and phase dependence of the intrinsic and extrinsic piezoelectric activity of domain engineered (1-x) $Pb(Mg_{1/3}Nb_{2/3})O_3$-x$PbTiO_3$ crystals", *J. Appl. Phys.*, **108** (2010) 034106.
36. D. Kobor, B. Guiffard, L. Lebrun, A. Hajjaji, D. Guyomar, "Oxygen vacancies effect on ionic conductivity and relaxation phenomenon in undoped and Mn doped PZN-4.5PT single crystals", *J. Phys. D Appl. Phys.*, **40** (2007) 2920–2926.
37. C. Wang, B. Fang, S. Zhang, X. Lu, J. Ding, "Doping effects in $(Ba_{0.85}Ca_{0.15})(Hf_{0.10}Ti_{0.90})O_3$ lead-free piezoelectric ceramics prepared via powder injection molding using simple binder", *Process. Appl. Ceram.*, **15** (2021) 47–57.
38. S. Wang, H. Zhang, T. Wang, C. Su, W. Hu, "Preparation, fluorescence and energy transfer mechanism of Eu^{3+}-Sm^{3+} co-doped glass ceramic containing $NaLa(MoO_4)_2$", *J. Non-Cryst. Solids*, **561** (2021) 120769.